



UvA-DARE (Digital Academic Repository)

Ferrocene-based light-responsive carbon nano hoops

Kręcijasz, R.B.

Publication date
2026

[Link to publication](#)

Citation for published version (APA):

Kręcijasz, R. B. (2026). *Ferrocene-based light-responsive carbon nano hoops*. [Thesis, fully internal, Universiteit van Amsterdam].

General rights

It is not permitted to download or to forward/distribute the text or part of it without the consent of the author(s) and/or copyright holder(s), other than for strictly personal, individual use, unless the work is under an open content license (like Creative Commons).

Disclaimer/Complaints regulations

If you believe that digital publication of certain material infringes any of your rights or (privacy) interests, please let the Library know, stating your reasons. In case of a legitimate complaint, the Library will make the material inaccessible and/or remove it from the website. Please Ask the Library: <https://uba.uva.nl/en/contact>, or a letter to: Library of the University of Amsterdam, Secretariat, P.O. Box 19185, 1000 GD Amsterdam, The Netherlands. You will be contacted as soon as possible.

1

Cycloparaphenylenes (CPPs) — Carbon Nanohoops

1.1 From graphite to CPPs

Carbon is an indispensable element and serves as a fundamental building block in organic chemistry. It is present in a wide range of compounds throughout the universe, from the interstellar medium to unicellular organisms, and can be found in over 95% of known chemical compounds,^[1] many of which are fundamental to modern technologies, such as synthetic polymers, pharmaceuticals and energy materials. The capacity of carbon to adopt various orbital hybridizations (sp , sp^2 , and sp^3) allows it to form stable covalent bonds not only with itself but also many other elements. As a result, carbon-based compounds display remarkable structural diversity and a wide range of physicochemical properties.

For a long time, carbon was known to exist in only two allotropic forms: diamond and graphite. Despite both being composed of pure carbon, they differ significantly in their crystal structures and physical properties. In the diamond form, each carbon atom is sp^3 -hybridized and covalently bonded to four other carbon atoms, creating a strong, three-dimensional network.^[2] This structure gives diamond its exceptional properties, including extreme hardness, high refractive index, excellent thermal conductivity, and very low electrical conductivity. These characteristics make diamond valuable for a range of industrial applications, such as abrasives, precision optical components, and heat spreaders in high-power electronic devices.^[3,4] In contrast, graphite consists of layers made up of sp^2 -hybridized carbon atoms. Within each layer, known as a graphene sheet, each carbon atom forms covalent bonds with three neighboring atoms, creating a flat, hexagonal lattice. These layers are held together by weak van der Waals interactions, with an interlayer spacing of 3.354 Å.^[5] As a result, the layers in graphite can easily slide over one another, giving it a soft and slippery texture, which makes it ideal for use in pencils and as a lubricant in electric motors.^[6] Additionally, graphite exhibits high thermal stability and excellent electrical and thermal conductivity, making it a suitable material for heat-resistant materials and electrodes.^[7]

In recent decades, several synthetic carbon allotropes have been discovered, including fullerenes,^[8] carbon nanotubes (CNTs),^[9] and graphene.^[10] Among these, graphene, a two-dimensional (2D) sheet of carbon atoms arranged in a hexagonal lattice, is perhaps the most emblematic, as many other carbon allotropes can be formally derived from it (Figure 1.1). Finite segments of graphene can be folded into structures that are classified according to the number of dimensions in which their unit cells repeat. For example, curving a segment into a spherical shape produces a fullerene, a zero-dimensional (0D) structure with no periodicity. Rolling it into a cylinder forms a carbon nanotube (CNT), a one-dimensional (1D) structure, while stacking multiple layers results in graphite, a three-dimensional (3D) material.

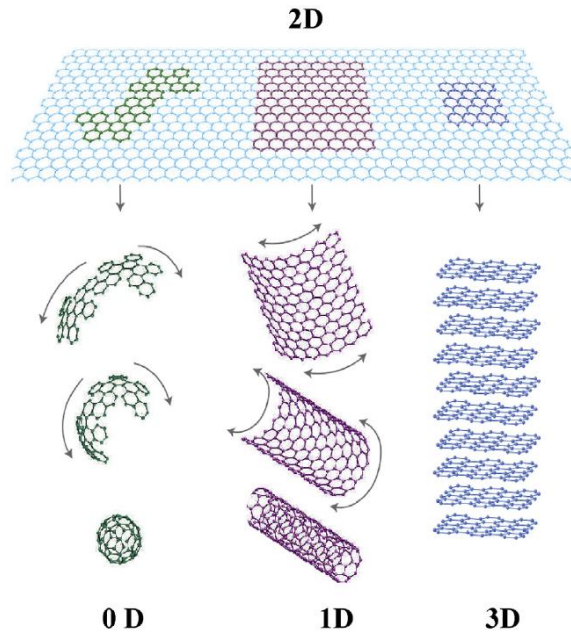


Figure 1.1. Graphene as a 2D material for carbon allotropes. It can be wrapped up into 0D fullerenes, rolled into 1D nanotubes, or layered into 3D graphite.^[11]

Since the first syntheses of CNTs in the early 1990s,^[9,12,13] this new carbon allotrope has rapidly found many applications in various areas such as composite materials, electronics, energy storage, sensors and biomaterials.^[14,15] In particular, due to their unique structure, CNTs exhibit several useful features such as high surface-to-volume ratio, tensile strength, light weight, electrical and thermal conductivity, and ability for functionalization. It is important to distinguish between single-walled CNTs (SWCNTs), which consist of a single cylindrical tube with diameters typically ranging from 0.4 to 2 nm, and multi-walled CNTs (MWCNTs), consisting of multiple cylinders stacked inside each other or wrapped like a scroll, with diameters often reaching tens of nanometers.^[16] While SWCNTs typically reach lengths in the micrometer range and MWCNTs can extend up to several millimeters, centimeter-scale CNTs of both types have also been successfully synthesized under optimized conditions.^[17,18]

A SWCNT can be further characterized by its chiral index (n,m) , where n and m are integers that define the vector along which a graphene sheet is virtually rolled to a SWCNT (Figure 1.2). When $n = m$, the nanotube is called “armchair”; if $n \neq 0$ and $m = 0$, it is called “zigzag”; if $n \neq m$ and $m \neq 0$, it is called “chiral”.^[19] The chiral index thus determines both the chirality and the diameter of a SWCNT. In contrast to the nanotube length, these two parameters strongly influence the chemical, mechanical^[20,21] and electronic^[22] properties of the material. To date, chemical vapor

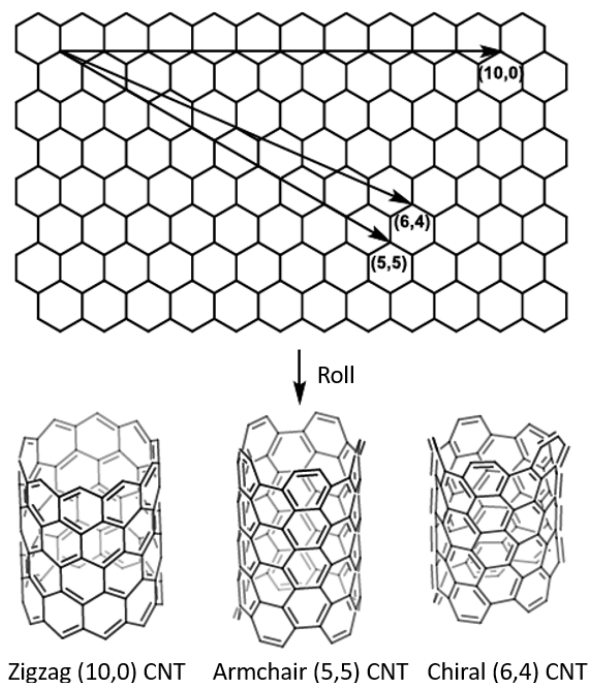


Figure 1.2. SWCNTs with different chirality as a result of rolling the graphene sheet with respect to specific vectors.

deposition (CVD) remains the most widely used method for synthesizing CNTs.^[15] This technique involves introducing a carbon-containing precursor gas into a reactor where it reacts with a substrate surface, leading to the gradual formation of CNTs.^[19] Other methods such as arc-discharge^[23] and laser ablation^[24] remain uncommon and high-energy routes. A major challenge in current CNT synthesis methods is the limited control over nanotube diameter and chirality, often resulting in heterogeneous mixtures that are difficult to separate. However, many applications require CNTs with precise structural characteristics to ensure optimal performance.

A promising strategy to address this challenge involves a bottom-up approach, in which a small molecule serves as a template to initiate the growth of CNTs. Under ideal conditions, extending a short CNT fragment with a defined diameter and structure should lead to the formation of uniform CNTs.^[25] For armchair nanotubes, such a template corresponds to the shortest lateral section of the tube, known as a cycloparaphenylene (CPP) or a carbon nano hoop (Figure 1.3a). By definition, $[n]$ CPPs are macrocyclic compounds composed solely of phenylene rings linked in *para* position.^[26] As the central subject of this thesis, the synthesis, properties, and applications of carbon nano hoops are discussed in detail below. Although not directly relevant in this work, it is worth mentioning the structural analog of zigzag CNTs: the $[n]$ cyclacene (Figure 1.3b). Despite

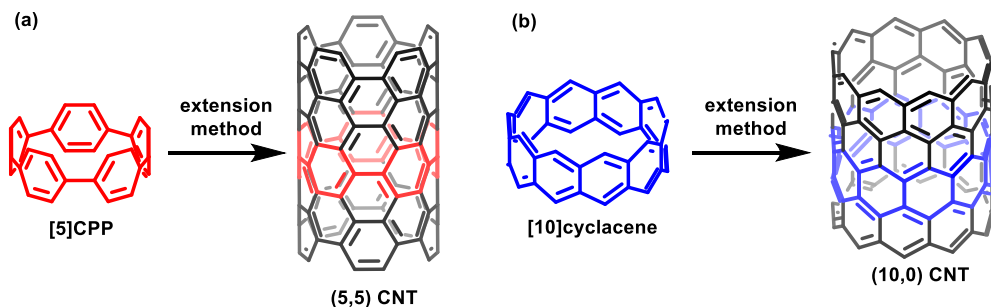


Figure 1.3. Bottom-up synthesis of (a) an armchair SWCNT from a $[n]$ cycloparaphenylene (b) a zigzag SWCNT from a $[n]$ cyclacene.^[26]

extensive efforts, the isolation of the latter has yet not been reported;^[27,28] however, the field has recently experienced a resurgence with diverse reports of zigzag-type belts incorporating non-hexagonal carbocyclic rings,^[29] heterocyclic rings,^[30] and various functional groups.^[31]

1.2 Synthesis of CPPs

Owing to their particular structure, CPPs were considered highly sought-after synthetic targets for a long time. Indeed, the main challenge lays in overcoming the high strain energy associated with bending the phenylene units, which naturally prefer a planar conformation, into a macrocyclic structure. The first successful synthesis of CPPs was achieved by Jasti and Bertozzi in 2008 (Figure 1.4a).^[26] Their method relies on using 1,4-*syn*-dimethoxy-2,5-cyclohexadienes as masked phenyl rings. The cyclohexadiene moiety provides the curvature necessary for the assembly of the macrocycle through Suzuki-Miyaura cross-coupling, allowing thus to circumvent the buildup of the strain. In the following step, the bent units undergo the aromatization through a two-electron reduction using sodium naphthalenide at -78 °C to yield the desired CPP. This approach was successfully applied for the size-selective synthesis of [5]–[12]CPPs.^[32–36] However, the strong reducing conditions and low temperature required to remove robust methoxy groups render this approach impractical for large-scale production. In addition, these conditions sometimes failed to achieve aromatization in the synthesis of highly strained nano hoops.^[36] To address these challenges, Yamago et al. developed an alternative approach using readily cleavable triethylsilyl (TES) groups and milder aromatization conditions, such as H_2SnCl_4 .^[37,38] Owing to its high yields and efficiency, even in the synthesis of highly strained nano hoops, this modification is now widely employed for the preparation of CPPs.

In 2009, Itami et al. developed a similar method wherein the low strain pro-aromatic macrocycles are obtained using 1,4-*syn*-diarylcyclohexane units as masked phenyl rings (Figure 1.4b).^[39] In

contrast to Jasti and Bertozzi's strategy, the final aromatization step can be achieved via an acid-mediated dehydration and subsequent oxidation (*e.g.*, using *p*-toluenesulfonic acid at 150 °C). This strategy enabled the size-selective synthesis of [7]–[16]CPPs.^[40–42] Shortly after, in 2010, a conceptually different approach was proposed by Yamago et al. (Figure 1.4c).^[43] Their method requires the use of platinum complexes, which upon reaction with aryl substrates (*e.g.*, aryl stannanes) provide low-strain square or tetragonal macrocycles. Typically in the presence of bromine, the latter then undergo reductive elimination to the corresponding CPPs. This strategy, characterized by a short number of synthetic steps and high yields, was successfully applied in the synthesis of [6]CPP and [8]–[13]CPPs.^[37,44–46] More recently, in 2020, Osakada et al. proposed another strategy relying on metal complexes (Figure 1.4d). In this method, the reaction of gold complexes with aryl boronic acids results in formation of triangular macrocycles, which upon oxidation in the final step afforded [6], [9], [12] and [15]CPPs.^[47,48] Remarkably, this approach requires few reaction steps and allows for the recovery of the starting gold complex.

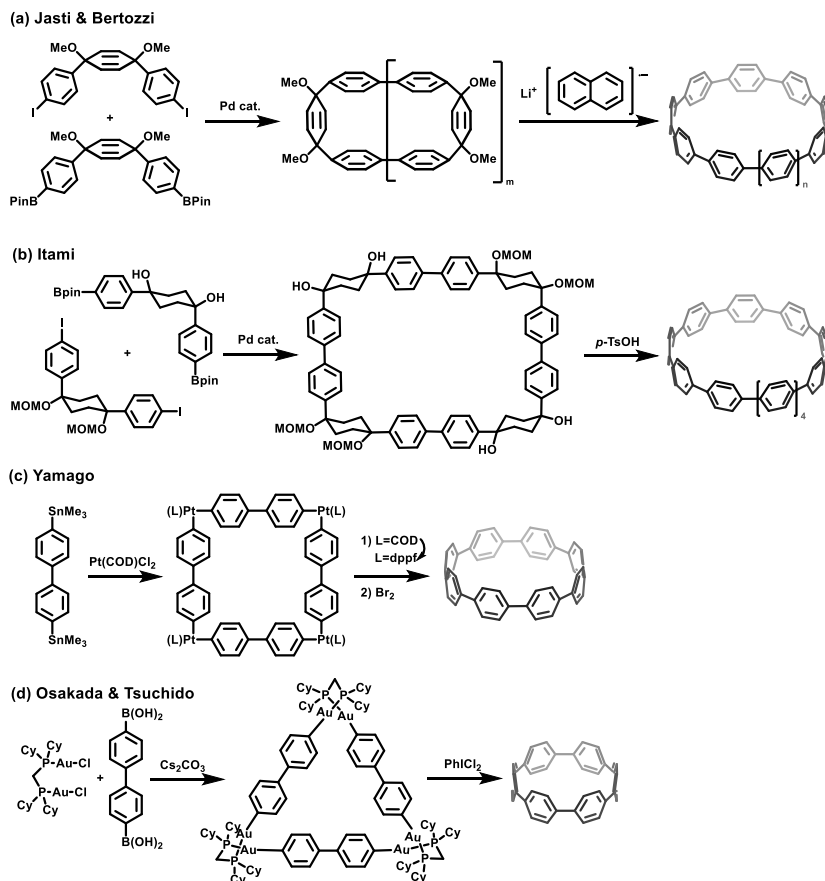


Figure 1.4. Overview of general synthetic methods to access CPPs.

1.3 Properties of CPPs

1.3.1 Structural properties

The properties of CPPs arise from the remarkable interplay of strain, geometry, and symmetry. As expected, strain energy increases with decreasing nanohoop size (Table 1.1). According to the calculations performed by the group of Itami, the strain energy increases from 48 kcal/mol for [12]CPP up to 119 kcal/mol for [5]CPP.^[49] As shown by DFT calculations, this significant buildup of strain has consequences on the geometry and conformation of CPPs.^[49–52] As the nanohoop size becomes smaller, the dihedral angle θ between adjacent phenylenes decreases to alleviate the rising strain.^[50,51] While larger [n]CPPs ($n > 12$) exhibit a constant average dihedral angle of approximately 35° , the angle progressively decreases along the series, reaching as low as 16° in [5]CPP,^[51] highlighting the unique structural characteristics of smaller nanohoops (Figure 1.5). The reduced dihedral angle enhances π -orbital overlap and the conjugation in smaller CPPs. In contrast, the dihedral angle observed in larger CPPs closely matches that of linear paraphenylenes ($\sim 36^\circ$), which maintain a similar value regardless of chain length, likely reflecting an optimal compromise between minimizing steric C–H interactions and maximizing π -conjugation.^[51] Additionally, the conformation of CPPs depends on whether the nanohoop contains an even or odd number of phenylenes.^[45] Even-numbered CPPs adopt $D_{(n/2)h}$ symmetry, characterized by uniform dihedral angles and an alternating canted orientation of the aryl rings across the structure.^[51] In contrast, odd-numbered CPPs exhibit C_2 symmetry, resulting in a distribution of dihedral angles around the hoop. Further structural details of [n]CPPs were revealed through analysis of their crystal structures.^[33,34,36,37,40,42,44,53] The average deviation of phenylene rings from planarity increases progressively, from 6.2° in [12]CPP to 15.8° ^[36] in [5]CPP (see ring displacement angle γ , Table 1.1). It was hypothesized that this pronounced bending of phenylenes in smaller nanohoops may reduce π -electron delocalization, potentially diminishing

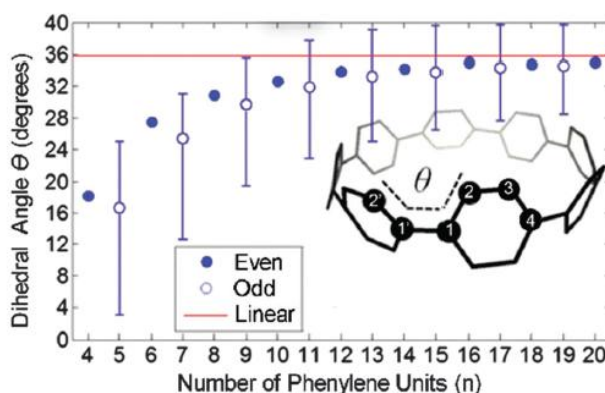



Figure 1.5. Calculated dihedral angle θ of cyclic (dots) and linear (red line) paraphenylenes.^[51]

Table 1.1. Structural, electrochemical and optical properties of [5]–[12]CPPs.

[n]CPP	Calculated strain (kcal mol ⁻¹)	Dihedral angle $\theta^{(51)}$ (°)	Average ring displacement angle γ (°)	Oxidation (V) vs. Fc/Fc ⁺	Reduction (V) vs. Fc/Fc ⁺	Absorbance (nm)	Extinction coefficient ϵ (M ⁻¹ cm ⁻¹)	Fluorescence (nm)	Fluorescence quantum yield ϕ
									
5	119 ^[36]	3 – 25	15.8 ^[36]	0.25, ^[36] 0.46 ^[36] 0.13, ^[37] 0.27 ^[37]	-2.27, ^[36] -2.55 ^[36] -1.59, ^[37] -1.91 ^[37]	335 ^[36,37]	5.7 × 10 ⁴ ^[36]	No fluorescence ^[36,37]	0 ^[36,37]
6	97 ^[49]	27	12.6 ^[33]	0.44, ^[33] 0.29 ^[46]	-	338 ^[33]	-	No fluorescence ^[33]	0 ^[33]
7	84 ^[49]	12 – 31	10.9 ^[42]	0.55, ^[52] 0.54 ^[55]	-2.74 ^[52]	339 ^[32]	6.9 × 10 ⁴ ^[52]	592 ^[32]	0.007 ^[32]
8	72 ^[49]	31	9.3 ^[34]	0.59, ^[45] 0.66 ^[55]	-	340 ^[43]	1.0 × 10 ⁵ ^[45]	540 ^[43]	0.10 ^[35]
9	66 ^[49]	20 – 36	8.3 ^[56]	0.70, ^[45] 0.72 ^[55]	-	341 ^[45]	1.2 × 10 ⁵ ^[45]	494 ^[45]	0.38 ^[35]
10	58 ^[49]	32	7.7 ^[44]	0.74, ^[45] 0.78 ^[55]	-	341 ^[45]	1.3 × 10 ⁵ ^[45]	466 ^[45]	0.65 ^[35]
11	54 ^[49]	23 – 38	6.8 ^[53]	0.83, ^[45] 0.83 ^[55]	-	340 ^[45]	1.3 × 10 ⁵ ^[45]	458 ^[45]	0.73 ^[35]
12	48 ^[49]	34	6.2 ^[40]	0.85, ^[45] 0.87 ^[55]	-	339 ^[45]	1.4 × 10 ⁵ ^[45]	450 ^[45]	0.81 ^[35]

aromatic character.^[54] Nevertheless, solid-state structural analysis of [5]CPP showed that all bond lengths within the phenylene rings remain nearly equivalent,^[36] indicating the preservation of a benzenoid rather than a quinoidal structure.

1.3.2 Electrochemical properties

Oxidation potentials of [5]–[12]CPPs, as well as reduction potentials of [5]CPP and [7]CPP, have been reported in the literature (Table 1.1).^[33,36,37,45,46,52,55] Notably, as observed by cyclic voltammetry (CV) and differential pulse voltammetry (DPV), the oxidation of CPPs becomes easier as the nanothoop size decreases, suggesting a rise in HOMO energy. For instance, the oxidation potential under identical conditions shifts from 0.87 V vs. Fc/Fc⁺ for [12]CPP to 0.54 V vs. Fc/Fc⁺ for [7]CPP.^[55] Similarly, the reduction also becomes more favorable in smaller nanothoops, indicating a lowering of LUMO energy.^[36,52] Together, these findings provide strong evidence for the elevation of HOMO and the lowering of LUMO energy levels with decreasing nanothoop size (Figure 1.6).

Interestingly, while [7]–[12]CPPs show a single reversible oxidation,^[45,52] [6]CPP displays a single quasi-reversible wave in CV with an atypically large separation between the anodic peak potential (E_{pa}) and cathodic peak potential (E_{pc}) (Figure 1.7a).^[33,46] On the contrary, [5]CPP exhibits two pseudo-reversible oxidations which were attributed to the formation of radical cation and dication.^[36,37] Although reduction potentials have been less intensively studied, [5]CPP also features two pseudo-reversible reductions, in contrast to [7]CPP which displays only one reversible reduction.^[36,37,52] According to Yamago et al., the single wave observed in CV for [6]–

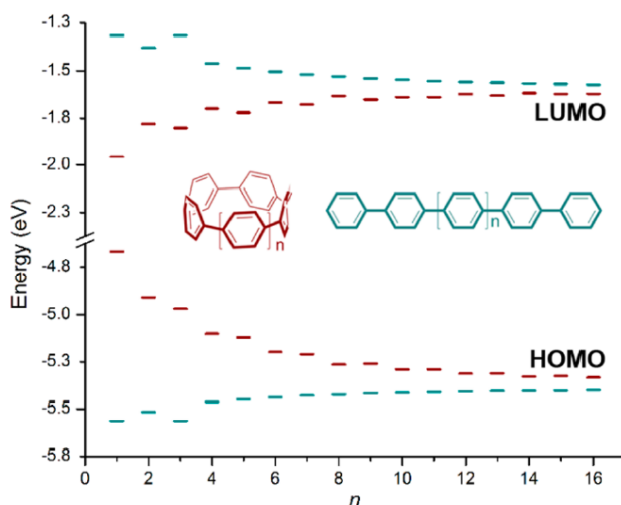


Figure 1.6. Calculated (B3LYP/6-31G*) HOMO and LUMO levels of cyclic (red) and linear (blue) *p*-phenylenes.^[56]

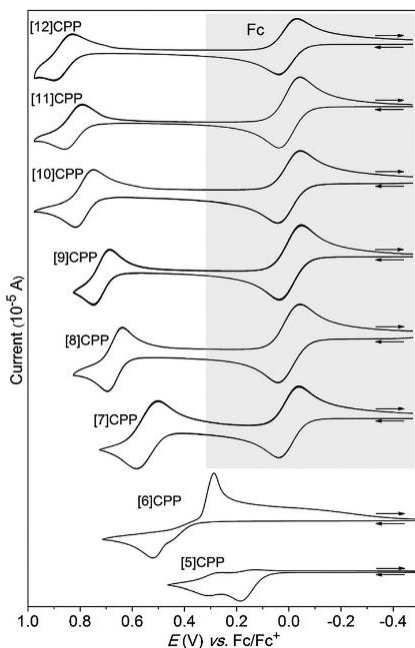


Figure 1.7. (a) Cyclic voltammograms of [5]–[12]CPPs (0.5 mM) in 0.1 M TBAPF₆/1,2-dichloroethane at a scan rate of $v = 100 \text{ mV s}^{-1}$, in the presence of equimolar ferrocene (Fc) except for [5]CPP and [6]CPP.^[55]

[12]CPPs corresponds to a two-electron process, and the difference between the first and second oxidation potentials becomes larger in smaller nano hoops.^[55] The first single-electron oxidation to the radical cation occurs more readily in smaller CPPs due to their higher HOMO energy. In contrast, the second single-electron oxidation to the dication is more favorable in larger CPPs, a trend attributed to the singly occupied molecular orbital (SOMO) in the radical cations. Indeed, the SOMO energy follows an opposite trend to the HOMO energy and increases with nano hoop size.^[57]

The chemical oxidation of [n]CPPs ($n = 5, 6, 8, 10, 12$) to the corresponding radical cations and dications was successfully achieved in good yields using oxidants such as NOSbF₆ and SbF₅.^[57,58] In comparison to the neutral CPPs, both oxidized species display UV–vis–NIR absorption bands with a significant bathochromic shift which increases with the nano hoop size. This size-dependance is in agreement with HOMO–SOMO and HOMO–LUMO gaps becoming narrower in larger CPPs^{•+} and CPPs²⁺, respectively. These results indicate enhanced in-plane π -conjugation and stronger polyene character in larger oxidized species.^[57] As demonstrated by ESR and NMR measurements, both the spin and charge of the oxidized species are completely delocalized across the *p*-phenylene framework.^[57] The redox behavior of CPPs contrasts with that

of linear paraphenylenes, which undergo only a one-electron oxidation to a radical cation.^[59] A possible explanation for the two-electron oxidation of CPPs can be the high stability of the resulting dication, which arises from the in-plane aromaticity enabled by the cyclic topology.^[60] $[n]$ CPPs can also undergo chemical reduction upon reaction with sodium or potassium metals, yielding the corresponding mono- ($n = 6$),^[61] di- ($n = 6, 8, 10, 12$)^[61,62] or tetra- ($n = 8$)^[63,64] anions. Structural analysis of the resulting dianions revealed an enhanced quinoidal character, particularly pronounced in the smaller $[6]$ CPP²⁻.^[62] In contrast, the tetra-reduced $[8]$ CPP⁴⁻ displayed a mixed benzenoid/quinoidal character.^[64] Reduction of CPPs also led to considerable elliptical distortion of the macrocyclic core, with the effect becoming more significant in larger CPPs. Computational studies attributed this structural deformation to the internal coordination of potassium cations within the nanohoop cavity, highlighting the potential of reduced CPPs for host–guest chemistry.

1.3.3 Optoelectronic properties

As a result of their topology, CPPs display interesting photophysical properties. The absorption spectra of $[5]$ – $[12]$ CPPs feature a typical profile with a common absorption maximum at 335–340 nm and a shoulder band at ~400 nm which shifts to higher energies with decreasing nanohoop size (Figure 1.8). Yamago and co-workers proposed an explanation for this phenomenon using time-dependent density functional theory (TD-DFT).^[45] In CPPs, both the HOMO and LUMO are delocalized symmetrically across all the phenylene units in the macrocycle, exhibiting overall centrosymmetry. Because the Laporte rule states that transitions between orbitals that are each symmetric with respect to an inversion centre are forbidden, the HOMO→LUMO transition exhibits zero oscillator strength in even-numbered nanohoops and only weak oscillator strength in odd-numbered ones.^[50] Further TD-DFT calculations revealed that $[5]$ – $[12]$ CPPs possess degenerate HOMO–1/HOMO–2 and nearly degenerate LUMO+1/LUMO+2 orbitals. Because these orbitals differ in symmetry from the HOMO and LUMO, the HOMO–1/HOMO–2→LUMO and HOMO→LUMO+1/LUMO+2 transitions are symmetry-allowed and have been assigned to the characteristic absorption band of $[5]$ – $[12]$ CPPs observed at 335–340 nm. The conservation of the common absorption across the series is further explained by the relative orbital energies: while the HOMO–LUMO gap increases with nanohoop size, the energy gap between HOMO–1/HOMO–2 and LUMO+1/LUMO+2 decreases (Figure 1.9). Notably, this trend is the opposite of what is typically observed in linear paraphenylenes and other conjugated systems, where the HOMO–LUMO gap narrows with increasing molecular size (Figure 1.6).^[65]

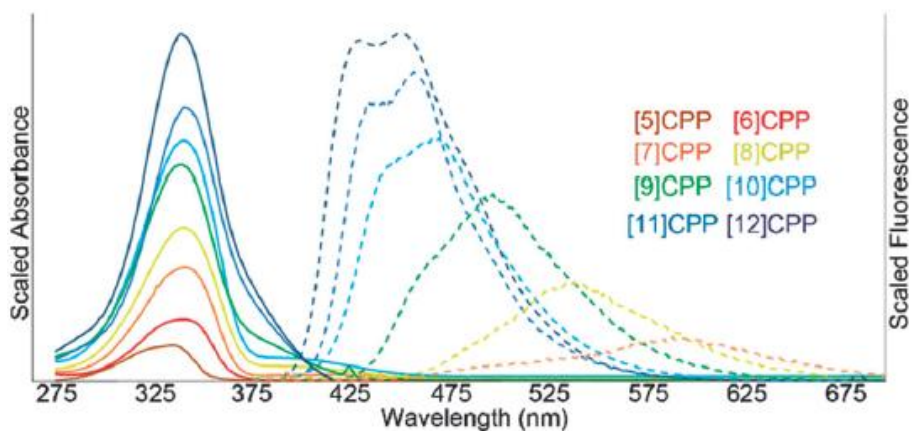


Figure 1.8. (a) UV-vis (solid line) and fluorescence (dashed line) of [5]–[12]CPPs. No fluorescence was observed for [5]CPP and [6]CPP.^[53]

In contrast to the absorption, the fluorescence of CPPs is strongly size-dependent. As the nanohoop size decreases, the emission undergoes a red shift and the quantum yield drops significantly, with [5]CPP and [6]CPP becoming essentially non-emissive (Figure 1.8, Table 1.1). According to Kasha's rule, fluorescence occurs from the lowest excited singlet state (S_1) to the ground state (S_0). However, due to the Laporte rule, initial excitation in CPPs primarily populates higher excited states such as S_2 and S_3 .^[45,50] Tretiak et al. demonstrated that these photoexcited states can undergo a rapid internal conversion within 50 femtoseconds to the spatially localized excited state S_1 .^[66] Importantly, in larger [n]CPPs ($n \geq 8$), the S_1 excited-state geometry exhibits partial planarization of five aryl rings, while the rest of the nanohoop remains in a geometry similar to that in the ground-state. This enables self-trapping of the exciton and leads to a symmetry change that makes the $S_1 \rightarrow S_0$ transition allowed. In contrast, smaller [n]CPPs ($n \leq 7$) display a fully delocalized S_1 state that retains ground-state symmetry, rendering the $S_1 \rightarrow S_0$ transition Laporte-forbidden and contributing to their lower quantum efficiencies.^[66]

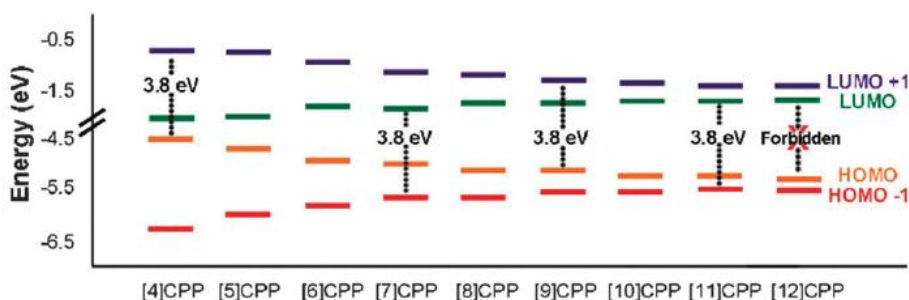


Figure 1.9. Calculated (B3LYP/6-31G*) HOMO, HOMO–1, LUMO, and LUMO+1 energy levels.^[53]

1.4 Applications of CPPs

1.4.1 General applications

The structural and photophysical properties of CPPs prompted the scientists to explore their potential across a range of applications. One of the most compelling and long-envisioned uses is their role as molecular seeds for the bottom-up synthesis of armchair SWCNTs. This concept was experimentally tested by Itami's group, who subjected [9]CPP and [12]CPP to chemical vapor deposition (CVD) using ethanol as the carbon source at 500 °C.^[67] While some of the resulting nanotubes displayed diameters closely matching those of the CPP precursors, precise control over chirality remained unsuccessful potentially due to the partial thermal decomposition of CPPs. Several other CPP derivatives incorporating substituted phenyl rings (e.g., tetraphenylbenzene^[68–71]), polycyclic aromatic hydrocarbons (e.g., naphthalene,^[72,73] pyrene,^[74,75] chrysenes^[76]) or exhibiting a dimeric structure^[77,78] were reported as alternative potential seeds for synthesis of SWCNTs (Figure 1.10a). Among these, tetraphenyl-substituted CPPs were particularly investigated for their potential to convert into the corresponding carbon nanobelts through cyclodehydrogenation, however these attempts proved unsuccessful.^[68–71] Despite the limited utility of CPPs in precise preparation of SWCNTs, carboxylated^[79] and fluorinated^[80–83] CPPs were shown to efficiently undergo self-assembly to tubular structures resembling CNTs (Figure 1.10b). The formation of these non-covalent CNTs was attributed to hydrogen bonding and arene–perfluoroarene interactions.

The intrinsic brightness, tunable emission, and large Stokes shifts of CPPs make them interesting scaffolds for various applications. In order to serve as fluorescent probes, the solubility of CPPs in aqueous mediums was achieved through functionalization with sulfonate^[84] or PEG^[85] groups (Figure 1.11a). Remarkably, the water-soluble nano hoops demonstrated good cell permeability and no cytotoxicity at concentrations of up to 50 μM , producing bright fluorescent in live-cell imaging. Furthermore, functionalization of the nano hoops with a clickable handle enabled derivatization with various groups, thereby allowing targeted live-cell imaging.^[84,85] More recently, oxidation of the non-fluorescent [5]CPP in air resulted in formation of blue-emissive aggregates,

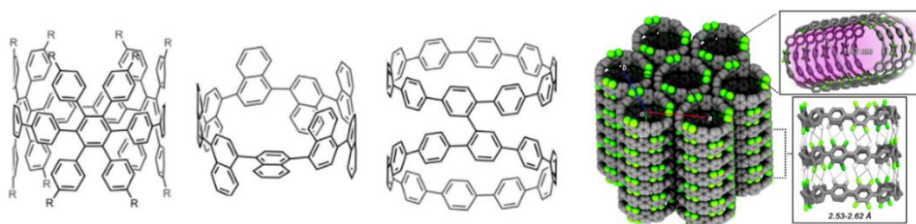


Figure 1.10. (a) Examples of armchair CPP derivatives.^[69,72,78] (b) X-ray crystal structure of fluorinated [12]CPP upon self-assembly into non-covalent CNT.^[81]

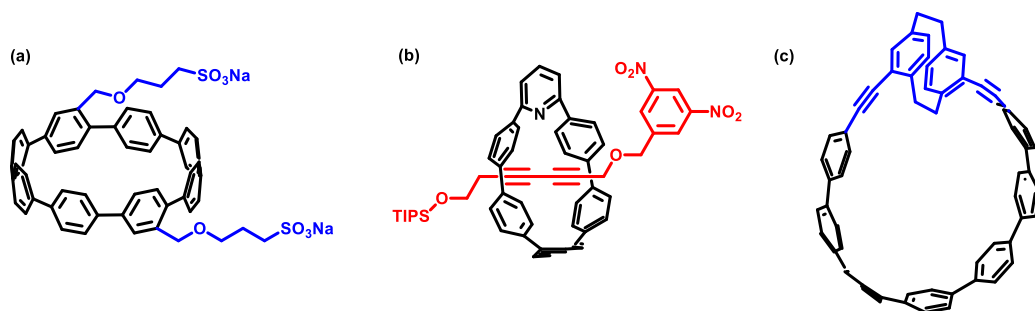


Figure 1.11. (a) Sulfonate-functionalized water soluble CPP for bio-imaging.^[84] (b) Nanohoop-based rotaxane for fluoride sensing.^[86] (c) [2,2]paracyclophane-containing CPP exhibiting CPL.^[87]

which, when encapsulated in liposomal nanoparticles, exhibited notable biocompatibility and imaging properties in cells.^[88] The emission of CPPs can also be applied to create efficient fluorescent sensors.^[86,89–91] For instance, the fluorescence from the nanohoop is fully quenched in the rotaxane form depicted in Figure 1.11b, however the addition of a fluoride source removes the triisopropylsilyl (TIPS) stopper, resulting in dethreading and a >100-fold increase in emission intensity.^[86] CPPs containing chiral moieties such as binaphthyl,^[92] [2,2]paracyclophane^[87,93] or helicene,^[94,95] have been shown to exhibit circularly polarized luminescence (CPL), which is of interest for applications in 3D displays, security encryption, and asymmetric synthesis. Furthermore, in contrast to many organic fluorophores, CPPs retain the bright emission in the solid state,^[50] making them suitable for solid-state optoelectronic applications such as electric-stimuli-responsive materials^[96] and luminescent solar concentrators.^[97]

Owing to their cyclic structure, CPPs are excellent candidates for host–guest chemistry. As electron-rich macrocycles, they readily accommodate electron-deficient guests such as fullerenes. Notably, among various nanohoop sizes, [10]CPP selectively binds the fullerene C₆₀ with a high binding constant ($K_a = 2.79 \times 10^6 \text{ M}^{-1}$ in toluene) (Figure 1.12a).^[98] This binding arises from a nearly perfect match in size and shape, further stabilized by convex–concave π – π interactions. Moreover, the formation of the [10]CPP \supset C₆₀ complex results in a significant quenching of [10]CPP fluorescence, suggesting potential sensing applications. Remarkably, the oval-shaped C₇₀ fullerene was found to be selectively encapsulated by [10]CPP in a standing orientation and by [11]CPP in a lying orientation.^[99] Several other studies expanded the scope of CPP \supset fullerene host–guest chemistry by including metallofullerenes,^[100,101] extending the π -surface of the nanohoop^[102,103] or functionalizing the nanohoop with a specific group such as porphyrin (Figure 1.12b–d).^[104] These approaches generally result in enhanced charge transfer

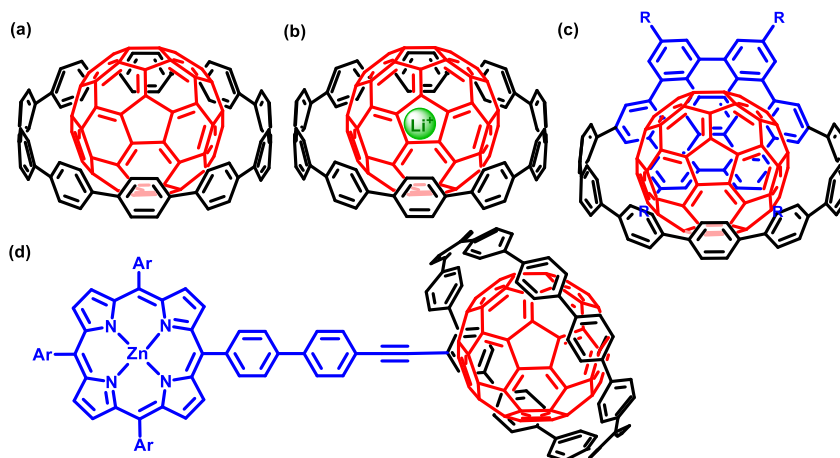


Figure 1.12. Examples of complexes of carbon nanohoops with fullerenes: (a) [10]CPP⊃C₆₀^[98] (b) [10]CPP⊃metallofullerene^[101] (c) extended π -surface CPP ⊃C₆₀^[102] (d) porphyrin functionalized CPP ⊃C₆₀^[104]

to the fullerene, making the CPPs interesting for use in supramolecular photovoltaic systems.^[102] Furthermore, the extraordinary features of CPPs make them promising candidates for many other interesting applications including organic electronics,^[105–108] porous sorption materials,^[109–111] optoelectronic devices,^[112–114] self-assembly of functional biomaterials,^[115] and supramolecular^[116] and stimuli-responsive^[117] materials.

1.4.2 Molecular shape control

A promising direction for future research is the control of the nanohoop shape and flexibility, for example to create stimuli-responsive materials or enable selective and reversible guest binding. Given the ability of CPPs to bind guests with specific sizes, such controlled uptake and release mechanisms could be particularly useful for separating mixtures of fullerenes or carbon nanotubes (CNTs) with different diameters. However, carbon nanohoops capable of shape modulation remain rare, with only a few examples reported in the literature.

Notably, in 2016, Cong's group synthesized a figure-eight-shaped nanohoop incorporating an anthracene photodimer as the central unit (Figure 1.13).^[118] Under optimized conditions involving heating at 175 °C in *o*-dichlorobenzene, the dianthracene core undergoes a cycloreversion reaction, resulting in ring expansion of the nanohoop. Although this transformation is not reversible, it provides access to a structurally distinct CPP derivative with interesting optical properties and potential applications in the bottom-up synthesis of carbon nanotubes.

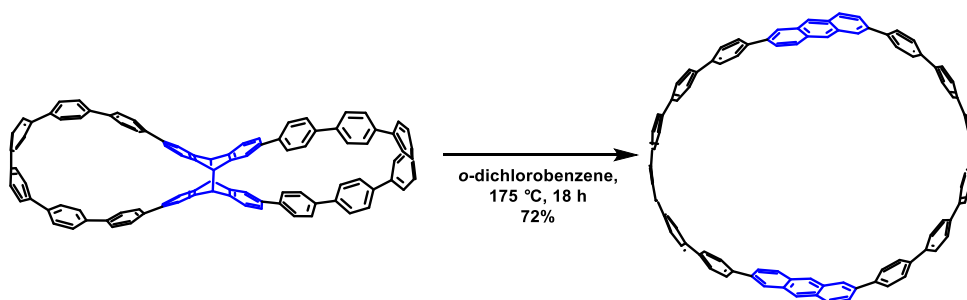


Figure 1.13. Cyclodimerization reaction of dianthracene figure-of-eight nano hoop.^[118]

In 2020, Stępień's group reported the synthesis of a novel hybrid macrocycle combining a paraphenylene loop with a calix[4]arene core, yielding a unique structure named the "molecular squid" (Figure 1.14).^[89] An automated conformational search followed by DFT optimization revealed that, despite significant strain energy, the oligophenylene loop can adopt either an elongated or circular geometry. This conformational flexibility arises from the calixarene unit, which switches between two non-equivalent flattened cone conformations. Consequently, the overall cavity of the structure can change between distinct shapes. This dynamic behavior was successfully applied to bind electron-deficient guests such as diquat, 10-methylacridinium, and anthraquinone. Moreover, the binding of guest molecules resulted in measurable changes in both absorbance and emission spectra, making the molecular squid promising for host-guest sensing applications.

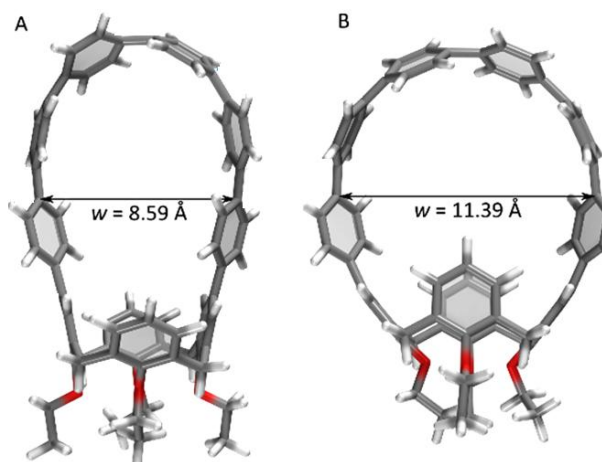


Figure 1.14. Lowest-energy elongated (A) and rounded (B) conformations (w = width of the loop) of molecular squid found in a gas-phase DFT calculation.^[89]

Another approach to control the curvature of CPPs involves the integration of a photoswitch directly into the macrocyclic backbone. To this end, nano hoops of different sizes incorporating either one^[119] or three^[120] azobenzene units as a photoswitch were successfully prepared in recent years (Figure 1.15a–b). All these compounds were found to adopt an all-*cis* conformation in both the solid state and in solution. Importantly, only the irradiation of the larger nano hoops resulted in reversible *cis-trans* isomerization, while the smaller nano hoops exhibited no photoresponsive behavior, most likely due to their higher strain energies. Remarkably, the treatment of the larger CPP embedding three azobenzene units (tris-azo[12]CPP) with excess trifluoroacetic acid led to the formation of the all-*trans* isomer, a transformation that could be reversed by the addition of triethylamine. This constitutes the first reported example of reversible interconversion between triangular and radial π -systems. However, the potential of these (photo)switchable macrocycles in host–guest applications has not been yet investigated.

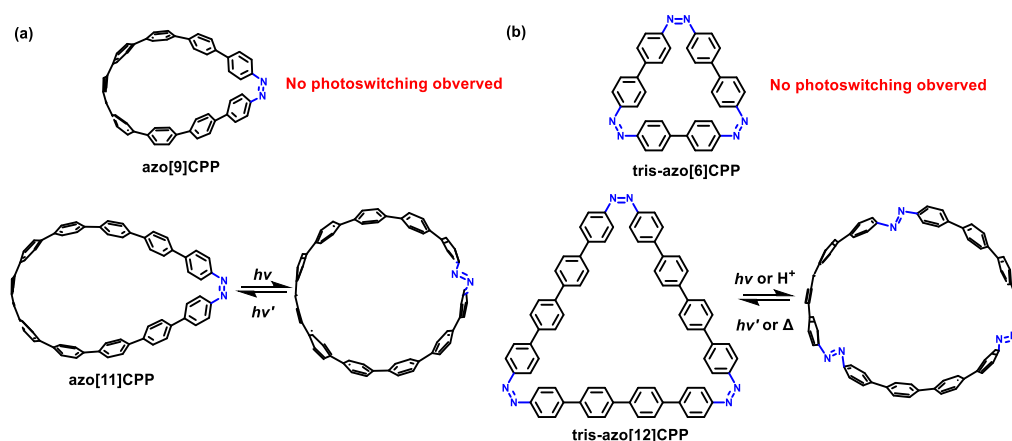


Figure 1.15. Structures of CPPs incorporating (a) one azobenzene moiety^[119] or (b) three azobenzene moieties.^[120]

The limited examples described above highlight that CPPs capable of undergoing (reversible) structural changes remain highly underexplored. To address this gap, the current thesis focuses on the synthesis and investigation of CPPs incorporating a novel moiety into the macrocyclic backbone: ferrocene. Due to its exceptional combination of structural and redox properties, good solubility in common organic solvents and stability in air, this metallocene has become widely applied in diverse areas, e.g., as a fuel additive to enhance performance,^[121,122] as a redox-active component in electrochemical sensors to detect various analytes,^[123,124] as a catalyst in diverse organic reactions,^[125,126] and as a material component of polymers and nanoparticles with electronic and magnetic properties.^[127,128] The success of ferrocene is further attributed to its chemical and photochemical robustness: consisting of an iron atom sandwiched between two

cyclopentadienyl (Cp) rings, ferrocene exhibits a relatively high Fe–Cp bond dissociation energy (BDE) of ~ 90 kcal mol⁻¹, which approaches that of a covalent C–C bond.^[129] Notably, both Cp rings possess a very low rotational energy barrier of 0.9 kcal mol⁻¹,^[130] allowing for nearly unrestricted rotation commonly referred to as “fluxionality.” Owing to this dynamic behavior, ferrocene functions effectively as a molecular bearing, enabling the synthesis of chemical structures capable of reversibly modifying the molecular shape.^[131–133] Incorporating ferrocene into the molecular backbone of CPPs thus gives access to an unprecedented class of π -conjugated metallamacrocycles, with potential relevance in the fields of responsive materials, and supramolecular and organometallic chemistry.

1.4.3 Metal-CPPs

Incorporating transition metals into CPPs provides a powerful strategy to tune their electronic properties^[90,134–138] and modulate their reactivity.^[134,135] As a distinct class of organometallic nano hoops, metal-CPPs hold significant promise for future advancements in organometallic chemistry, molecular electronics, and supramolecular chemistry. The following section reviews examples of metal-CPPs reported to this date.

In 2015, the group of Itami was the first one to merge CPPs with transition metals. According to their report, [9]CPP-Cr(CO)₃ was successfully isolated upon reaction of [9]CPP with Cr(CO)₆ at 160 °C, however only in moderate 35 % yield (Figure 1.16).^[134] NMR and X-ray crystallographic analyses confirmed that the chromium center coordinates in an η^6 fashion to a single phenylene unit on the convex face of [9]CPP. Remarkably, the authors demonstrated that the obtained complex can be used for a highly selective one-pot monofunctionalization of CPPs with groups such as silyl, boryl or methoxycarbonyl. This strategy effectively circumvents the issues related to common electrophilic substitution reactions performed on CPPs, which often lead to complex product mixtures, and thus offers a valuable tool for the preparation of new functional nanocarbons.

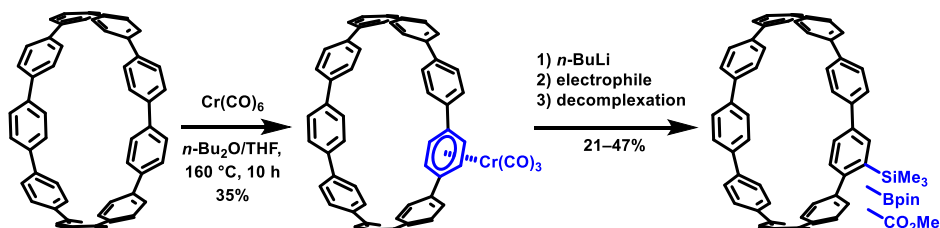


Figure 1.16. Complexation of [9]CPP with Cr(CO)₃, followed by monofunctionalization.^[134]

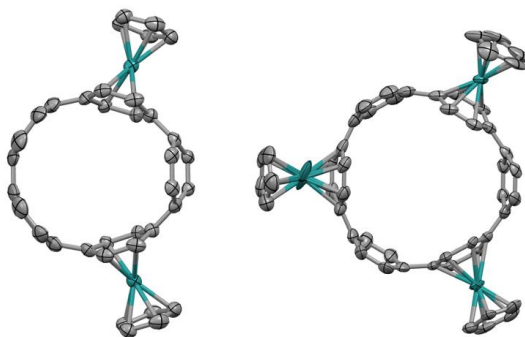


Figure 1.17. X-ray crystal structures of binuclear ruthenium [5]CPP (left) and trinuclear ruthenium [6]CPP (right) complexes. Gray: C, turquoise: Ru. Thermal ellipsoids shown at 50% probability. All hydrogen atoms, solvent molecules and PF_6^- were omitted for clarity.^[135]

In 2016, Yamago and co-workers reported the first synthesis of multinuclear transition-metal-CPP complexes via ligand exchange between the ruthenium complex $[(\text{Cp})\text{Ru}(\text{CH}_3\text{CN})_3](\text{PF}_6)$ with CPPs ($n = 5, 6$).^[135] Notably, the reaction afforded bis- and tris-ruthenium complexes from [5]CPP and [6]CPP, respectively, in excellent yields and with the metal selectively coordinated to alternate paraphenylene rings (Figure 1.17). The full regioselectivity of this reaction, combined with mild conditions and high yields, offers a useful strategy for the site-selective functionalization of CPPs. Interestingly, this behavior contrasts sharply with that of linear paraphenylenes, where ruthenium coordinates to all available phenylene rings,^[139] highlighting the special reactivity conferred by the cyclic topology of CPPs.

Although innovative, the approaches described above utilize CPPs only as η^6 -type ligands, limiting their versatility and broader applicability as a general ligand class. To address this, Jasti and co-workers developed a scalable method for synthesis of CPPs incorporating a 2,2'-bipyridine (bipy) unit, enabling bidentate coordination with a wide range of metals.^[136] For example, bipy-[8]CPP was successfully employed to prepare a palladium-centered nanohoop dimer and a bis(bipyridyl)ruthenium(II)-functionalized nanohoop (Figure 1.18a), both of which displayed notable photophysical properties.^[136] In a later study, bipy-[9]CPP was used to prepare an iron(II) complex, where the inherent non-planarity of the ligand led to spin-crossover behavior.^[137] More recently, Jasti's group introduced a new class of bidentate CPP-based ligands functionalized with polycatechol groups (Figure 1.18b).^[140] Remarkably, these nanohoops were successfully metalated with half-sandwich Ru(II) fragments to form well-defined multinuclear complexes. However, the metalation reactions proceeded in low yields, likely due to the oxidative sensitivity of the catechol-functionalized ligands. Despite this limitation, this emerging class of CPP ligands holds promise for development of extended metalloorganic architectures.

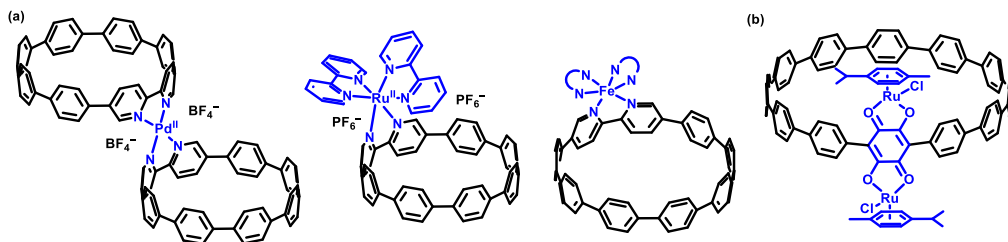


Figure 1.18. Reported metal complexes with (a) bipy-CPP^[136,137] or (b) polycatechol-CPP as bidentate ligands.^[140]

In 2024, Itami's group reported the syntheses of CPPs incorporating either one^[90] or three^[138] Fc units (Figure 1.19a). It is important to note that the metallocene within these structures is attached through a single Cp ring, and therefore the iron atom is not an integral part of the macrocycle. The resulting CPPs thus differ considerably from those described in this thesis. Interestingly, despite Fc's well-known fluorescence-quenching properties, CPPs bearing a single Fc moiety (Figure 1.19a) remained emissive, albeit with significantly reduced quantum yields compared to their metallocene-free analogues. Upon addition of an oxidizing agent, fluorescence intensity increased, supporting a photoinduced electron transfer (PET) mechanism by which Fc partially quenches emission.^[90] In contrast, the addition of fullerenes resulted in quenching of fluorescence. The reversible fluorescence response of these Fc -based nanohoops offers thus significant potential for use in multifunctional devices. Concerning the CPPs incorporating three Fc units,^[138] two stereoisomers were isolated: A₃, where all three Fc groups are oriented in the same direction relative to the ring plane, and A₂B, where one Fc group adopts an *anti*-orientation with respect to the other two (Figure 1.19b). Despite these structural differences, UV-vis spectroscopy and theoretical calculations indicated that the electronic properties of the conjugated systems are only minimally influenced by the orientation of the Fc moieties.

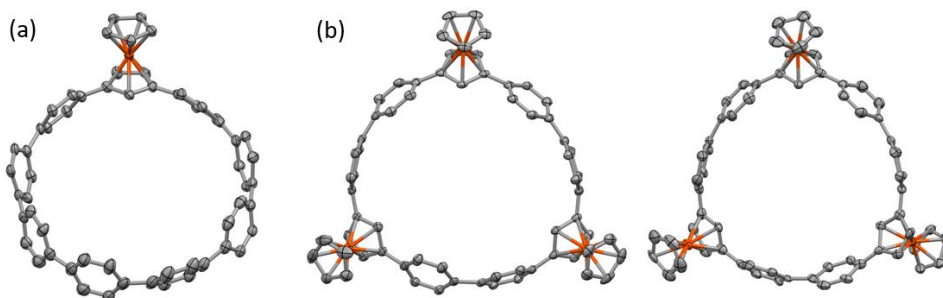


Figure 1.19. X-ray structures of CPPs incorporating (a) one Fc unit^[90] (b) three Fc units (stereoisomers).^[138] Gray: C, orange: Fe. Thermal ellipsoids shown at 50% probability. All hydrogen atoms and solvent molecules were omitted for clarity.

Furthermore, electrochemical studies revealed weak electronic communication between the redox-active centers, likely due to the significant spatial separation of the metal atoms. Consequently, the main interest in these nano hoops, yet unexplored, remains in their potential use as curved, π -conjugated macrocyclic ligands for coordination chemistry.

As outlined above, the field of CPPs has grown significantly since their first synthesis in 2008. Given the fascinating properties and potential applications of these nano hoops, the field continues to expand, necessitating new methodologies to access increasingly complex and synthetically challenging targets. In this thesis, an alternative silyl protecting group for the cyclohexadienyl unit, a commonly used curved building block in CPP synthesis, is proposed in Chapter 2. Chapter 3 describes the synthesis, characterization, and photochemical reactivity of the first CPP incorporating a fully embedded Fc unit, **Fc[6]CPP**. Chapter 4 presents a comparative study of various properties across a series of **Fc[n]CPPs** ($n = 6, 7, 8$), while Chapter 5 details the efforts toward isolating the smaller **Fc[5]CPP**. Finally, Chapter 6 reports the synthesis and characterization of two conformationally locked Fc-containing nanoscrolls: **a-Fc[6]CPP** and **a-Fc[8]CPP**.

1.5 References

- [1] E. H. Falcao, F. Wudl, *J. Chem. Technol. Biotechnol.* **2007**, *82*, 524–531.
- [2] W. H. Bragg, W. L. Bragg, *Proc. R. Soc. Lond. Ser. Contain. Pap. Math. Phys. Character* **1997**, *89*, 277–291.
- [3] J. Robertson, *Surf. Coat. Technol.* **1992**, *50*, 185–203.
- [4] O. A. Williams, *Diam. Relat. Mater.* **2011**, *20*, 621–640.
- [5] J. D. Bernal, W. L. Bragg, *Proc. R. Soc. Lond. Ser. Contain. Pap. Math. Phys. Character* **1997**, *106*, 749–773.
- [6] S. Nasir, M. Z. Hussein, Z. Zainal, N. A. Yusof, *Materials* **2018**, *11*, 295.
- [7] D. D. L. Chung, *J. Mater. Sci.* **2002**, *37*, 1475–1489.
- [8] H. W. Kroto, J. R. Heath, S. C. O'Brien, R. F. Curl, R. E. Smalley, *Nature* **1985**, *318*, 162–163.
- [9] S. Iijima, *Nature* **1991**, *354*, 56–58.
- [10] K. S. Novoselov, A. K. Geim, S. V. Morozov, D. Jiang, Y. Zhang, S. V. Dubonos, I. V. Grigorieva, A. A. Firsov, *Science* **2004**, *306*, 666–669.
- [11] A. K. Geim, K. S. Novoselov, *Nat. Mater.* **2007**, *6*, 183–191.
- [12] D. S. Bethune, C. H. Kiang, M. S. de Vries, G. Gorman, R. Savoy, J. Vazquez, R. Beyers, *Nature* **1993**, *363*, 605–607.
- [13] S. Iijima, T. Ichihashi, *Nature* **1993**, *363*, 603–605.
- [14] L. Sun, X. Wang, Y. Wang, Q. Zhang, *Carbon* **2017**, *122*, 462–474.
- [15] K. J. Hughes, K. A. Iyer, R. E. Bird, J. Ivanov, S. Banerjee, G. Georges, Q. A. Zhou, *ACS Appl. Nano Mater.* **2024**, *7*, 18695–18713.

- [16] A. Aqel, K. M. M. A. El-Nour, R. A. A. Ammar, A. Al-Warthan, *Arab. J. Chem.* **2012**, *5*, 1–23.
- [17] L. X. Zheng, M. J. O'Connell, S. K. Doorn, X. Z. Liao, Y. H. Zhao, E. A. Akhadorov, M. A. Hoffbauer, B. J. Roop, Q. X. Jia, R. C. Dye, D. E. Peterson, S. M. Huang, J. Liu, Y. T. Zhu, *Nat. Mater.* **2004**, *3*, 673–676.
- [18] Q. Wen, W. Qian, J. Nie, A. Cao, G. Ning, Y. Wang, L. Hu, Q. Zhang, J. Huang, F. Wei, *Adv. Mater.* **2010**, *22*, 1867–1871.
- [19] G. D. Nessim, *Nanoscale* **2010**, *2*, 1306–1323.
- [20] Q. Yuan, L. Li, Q. Li, F. Ding, *J. Phys. Chem. C* **2013**, *117*, 5470–5474.
- [21] L. Zhu, J. Wang, F. Ding, *ACS Nano* **2016**, *10*, 6410–6415.
- [22] M. He, S. Zhang, Q. Wu, H. Xue, B. Xin, D. Wang, J. Zhang, *Adv. Mater.* **2019**, *31*, 1800805.
- [23] T. W. Ebbesen, P. M. Ajayan, *Nature* **1992**, *358*, 220–222.
- [24] T. Guo, P. Nikolaev, A. Thess, D. T. Colbert, R. E. Smalley, *Chem. Phys. Lett.* **1995**, *243*, 49–54.
- [25] R. Jasti, C. R. Bertozzi, *Chem. Phys. Lett.* **2010**, *494*, 1–7.
- [26] R. Jasti, J. Bhattacharjee, J. B. Neaton, C. R. Bertozzi, *J. Am. Chem. Soc.* **2008**, *130*, 17646–17647.
- [27] T.-H. Shi, Q.-H. Guo, S. Tong, M.-X. Wang, *J. Am. Chem. Soc.* **2020**, *142*, 4576–4580.
- [28] T.-H. Shi, Q.-H. Guo, S. Tong, M.-X. Wang, *Acc. Chem. Res.* **2025**, DOI 10.1021/acs.accounts.5c00328.
- [29] Q. Zhang, Y.-E. Zhang, S. Tong, M.-X. Wang, *J. Am. Chem. Soc.* **2020**, *142*, 1196–1199.
- [30] M.-L. Tan, Q.-H. Guo, X.-Y. Wang, T.-H. Shi, Q. Zhang, S.-K. Hou, S. Tong, J. You, M.-X. Wang, *Angew. Chem. Int. Ed.* **2020**, *59*, 23649–23658.
- [31] Y. Zhang, S. Tong, M.-X. Wang, *Angew. Chem. Int. Ed.* **2020**, *59*, 18151–18155.
- [32] T. J. Sisto, M. R. Golder, E. S. Hirst, R. Jasti, *J. Am. Chem. Soc.* **2011**, *133*, 15800–15802.
- [33] J. Xia, R. Jasti, *Angew. Chem. Int. Ed.* **2012**, *51*, 2474–2476.
- [34] J. Xia, J. W. Bacon, R. Jasti, *Chem. Sci.* **2012**, *3*, 3018.
- [35] E. R. Darzi, T. J. Sisto, R. Jasti, *J. Org. Chem.* **2012**, *77*, 6624–6628.
- [36] P. J. Evans, E. R. Darzi, R. Jasti, *Nat. Chem.* **2014**, *6*, 404–408.
- [37] E. Kayahara, V. K. Patel, S. Yamago, *J. Am. Chem. Soc.* **2014**, *136*, 2284–2287.
- [38] V. K. Patel, E. Kayahara, S. Yamago, *Chem. – Eur. J.* **2015**, *21*, 5742–5749.
- [39] H. Takaba, H. Omachi, Y. Yamamoto, J. Bouffard, K. Itami, *Angew. Chem. Int. Ed.* **2009**, *48*, 6112–6116.
- [40] Y. Segawa, S. Miyamoto, H. Omachi, S. Matsuura, P. Šenel, T. Sasamori, N. Tokitoh, K. Itami, *Angew. Chem. Int. Ed.* **2011**, *50*, 3244–3248.
- [41] Y. Ishii, Y. Nakanishi, H. Omachi, S. Matsuura, K. Matsui, H. Shinohara, Y. Segawa, K. Itami, *Chem. Sci.* **2012**, *3*, 2340.
- [42] F. Sibbel, K. Matsui, Y. Segawa, A. Studer, K. Itami, *Chem Commun* **2014**, *50*, 954–956.
- [43] S. Yamago, Y. Watanabe, T. Iwamoto, *Angew. Chem. Int. Ed.* **2010**, *49*, 757–759.
- [44] E. Kayahara, Y. Sakamoto, T. Suzuki, S. Yamago, *Org. Lett.* **2012**, *14*, 3284–3287.
- [45] T. Iwamoto, Y. Watanabe, Y. Sakamoto, T. Suzuki, S. Yamago, *J. Am. Chem. Soc.* **2011**, *133*, 8354–8361.
- [46] E. Kayahara, T. Iwamoto, T. Suzuki, S. Yamago, *Chem. Lett.* **2013**, *42*, 621–623.
- [47] Y. Tsuchido, R. Abe, T. Ide, K. Osakada, *Angew. Chem.* **2020**, *132*, 23128–23132.
- [48] Y. Yoshigoe, Y. Tanji, Y. Hata, K. Osakada, S. Saito, E. Kayahara, S. Yamago, Y. Tsuchido, H. Kawai, *JACS Au* **2022**, *2*, 1857–1868.
- [49] Y. Segawa, H. Omachi, K. Itami, *Org. Lett.* **2010**, *12*, 2262–2265.

- [50] Y. Segawa, A. Fukazawa, S. Matsuura, H. Omachi, S. Yamaguchi, S. Irle, K. Itami, *Org. Biomol. Chem.* **2012**, *10*, 5979.
- [51] H. Chen, M. R. Golder, F. Wang, R. Jasti, A. K. Swan, *Carbon* **2014**, *67*, 203–213.
- [52] P. Li, T. J. Sisto, E. R. Darzi, R. Jasti, *Org. Lett.* **2014**, *16*, 182–185.
- [53] E. R. Darzi, R. Jasti, *Chem. Soc. Rev.* **2015**, *44*, 6401–6410.
- [54] M. N. Jagadeesh, A. Makur, J. Chandrasekhar, *Mol. Model. Annu.* **2000**, *6*, 226–233.
- [55] E. Kayahara, K. Fukayama, T. Nishinaga, S. Yamago, *Chem. – Asian J.* **2016**, *11*, 1793–1797.
- [56] M. R. Golder, R. Jasti, *Acc. Chem. Res.* **2015**, *48*, 557–566.
- [57] E. Kayahara, T. Kouyama, T. Kato, S. Yamago, *J. Am. Chem. Soc.* **2016**, *138*, 338–344.
- [58] E. Kayahara, T. Kouyama, T. Kato, H. Takaya, N. Yasuda, S. Yamago, *Angew. Chem. Int. Ed.* **2013**, *52*, 13722–13726.
- [59] M. R. Talipov, A. Boddeda, Q. K. Timerghazin, R. Rathore, *J. Phys. Chem. C* **2014**, *118*, 21400–21408.
- [60] N. Toriumi, A. Muranaka, E. Kayahara, S. Yamago, M. Uchiyama, *J Am Chem Soc* **2015**, *4*.
- [61] S. N. Spisak, Z. Wei, E. Darzi, R. Jasti, M. A. Petrukhina, *Chem. Commun.* **2018**, *54*, 7818–7821.
- [62] Z. Zhou, Z. Wei, T. A. Schaub, R. Jasti, M. A. Petrukhina, *Chem. Sci.* **2020**, *11*, 9395–9401.
- [63] A. V. Zabula, A. S. Filatov, J. Xia, R. Jasti, M. A. Petrukhina, *Angew. Chem. Int. Ed.* **2013**, *52*, 5033–5036.
- [64] A. Yu. Rogachev, Z. Zhou, S. Liu, Z. Wei, T. A. Schaub, R. Jasti, M. A. Petrukhina, *Chem. Sci.* **2021**, *10*.1039.D1SC00713K.
- [65] M. Banerjee, R. Shukla, R. Rathore, *J. Am. Chem. Soc.* **2009**, *131*, 1780–1786.
- [66] L. Adamska, I. Nayyar, H. Chen, A. K. Swan, N. Oldani, S. Fernandez-Alberti, M. R. Golder, R. Jasti, S. K. Doorn, S. Tretiak, *Nano Lett.* **2014**, *14*, 6539–6546.
- [67] H. Omachi, T. Nakayama, E. Takahashi, Y. Segawa, K. Itami, *Nat. Chem.* **2013**, *5*, 572–576.
- [68] T. J. Sisto, X. Tian, R. Jasti, *J. Org. Chem.* **2012**, *77*, 5857–5860.
- [69] T. Nishiuchi, X. Feng, V. Enkelmann, M. Wagner, K. Müllen, *Chem. – Eur. J.* **2012**, *18*, 16621–16625.
- [70] F. E. Golling, M. Quernheim, M. Wagner, T. Nishiuchi, K. Müllen, *Angew. Chem. Int. Ed.* **2014**, *53*, 1525–1528.
- [71] M. Quernheim, F. E. Golling, W. Zhang, M. Wagner, H.-J. Räder, T. Nishiuchi, K. Müllen, *Angew. Chem. Int. Ed.* **2015**, *54*, 10341–10346.
- [72] A. Yagi, Y. Segawa, K. Itami, *J. Am. Chem. Soc.* **2012**, *134*, 2962–2965.
- [73] J. M. Batson, T. M. Swager, *Synlett* **2013**, *24*, 2545–2549.
- [74] A. Yagi, G. Venkataramana, Y. Segawa, K. Itami, *Chem Commun* **2014**, *50*, 957–959.
- [75] T. Iwamoto, E. Kayahara, N. Yasuda, T. Suzuki, S. Yamago, *Angew. Chem. Int. Ed.* **2014**, *53*, 6430–6434.
- [76] S. Hitosugi, W. Nakanishi, T. Yamasaki, H. Isobe, *Nat. Commun.* **2011**, *2*, 492.
- [77] J. Xia, M. R. Golder, M. E. Foster, B. M. Wong, R. Jasti, *J. Am. Chem. Soc.* **2012**, *134*, 19709–19715.
- [78] Y. Ishii, S. Matsuura, Y. Segawa, K. Itami, *Org. Lett.* **2014**, *16*, 2174–2176.
- [79] Y. Miyauchi, K. Johmoto, N. Yasuda, H. Uekusa, S. Fujii, M. Kiguchi, H. Ito, K. Itami, K. Tanaka, *Chem. – Eur. J.* **2015**, *21*, 18900–18904.

- [80] S. Hashimoto, E. Kayahara, Y. Mizuhata, N. Tokitoh, K. Takeuchi, F. Ozawa, S. Yamago, *Org. Lett.* **2018**, *20*, 5973–5976.
- [81] E. J. Leonhardt, J. M. Van Raden, D. Miller, L. N. Zakharov, B. Alemán, R. Jasti, *Nano Lett.* **2018**, *18*, 7991–7997.
- [82] J. M. Van Raden, E. J. Leonhardt, L. N. Zakharov, A. Pérez-Guardiola, A. J. Pérez-Jiménez, C. R. Marshall, C. K. Brozek, J. C. Sancho-García, R. Jasti, *J. Org. Chem.* **2020**, *85*, 129–141.
- [83] H. Shudo, M. Kuwayama, M. Shimasaki, T. Nishihara, Y. Takeda, N. Mitoma, T. Kuwabara, A. Yagi, Y. Segawa, K. Itami, *Nat. Commun.* **2022**, *13*, 3713.
- [84] B. M. White, Y. Zhao, T. E. Kawashima, B. P. Branchaud, M. D. Pluth, R. Jasti, *ACS Cent. Sci.* **2018**, *4*, 1173–1178.
- [85] T. C. Lovell, S. G. Bolton, J. P. Kenison, J. Shangguan, C. E. Otteson, F. Civitci, X. Nan, M. D. Pluth, R. Jasti, *ACS Nano* **2021**, *15*, 15285–15293.
- [86] J. M. Van Raden, B. M. White, L. N. Zakharov, R. Jasti, *Angew. Chem. Int. Ed.* **2019**, *58*, 7341–7345.
- [87] J. He, M. Yu, M. Pang, Y. Fan, Z. Lian, Y. Wang, W. Wang, Y. Liu, H. Jiang, *Chem. – Eur. J.* **2022**, *28*, e202103832.
- [88] Y. K. Park, Y. Huh, D. Kim, *Dyes Pigments* **2023**, *211*, 111056.
- [89] R. Frydrych, T. Lis, W. Bury, J. Cybińska, M. Stępień, *J. Am. Chem. Soc.* **2020**, *142*, 15604–15613.
- [90] L. Zhu, J. Xu, B. Lan, X. Chen, H. Kono, H. Xu, J. Yan, W. Li, A. Yagi, Y. Yuan, K. Itami, Y. Li, *Org. Chem. Front.* **2024**, *11*, 5130–5137.
- [91] Y. Fan, J. He, L. Liu, G. Liu, S. Guo, Z. Lian, X. Li, W. Guo, X. Chen, Y. Wang, H. Jiang, *Angew. Chem.* **2023**, *135*, e202304623.
- [92] K. Sato, M. Hasegawa, Y. Nojima, N. Hara, T. Nishiuchi, Y. Imai, Y. Mazaki, *Chem. – Eur. J.* **2021**, *27*, 1323–1329.
- [93] K. Kovida, J. Malinčík, C. M. Cruz, A. G. Campaña, T. Šolomek, *Chem. Sci.* **2025**, *16*, 1405–1410.
- [94] K. Kovida, J. Malinčík, T. Šolomek, *Helv. Chim. Acta* **2025**, *108*, e202400166.
- [95] J. Malinčík, S. Gaikwad, J. P. Mora-Fuentes, M.-A. Boillat, A. Prescimone, D. Häussinger, A. G. Campaña, T. Šolomek, *Angew. Chem. Int. Ed.* **2022**, *61*, e202208591.
- [96] N. Ozaki, H. Sakamoto, T. Nishihara, T. Fujimori, Y. Hijikata, R. Kimura, S. Irle, K. Itami, *Angew. Chem. Int. Ed.* **2017**, *56*, 11196–11202.
- [97] P. D. Sala, N. Buccheri, A. Sanzone, M. Sassi, P. Neri, C. Talotta, A. Rocco, V. Pinchetti, L. Beverina, S. Brovelli, C. Gaeta, *Chem. Commun.* **2019**, *55*, 3160–3163.
- [98] T. Iwamoto, Y. Watanabe, T. Sadahiro, T. Haino, S. Yamago, *Angew. Chem. Int. Ed.* **2011**, *50*, 8342–8344.
- [99] T. Iwamoto, Y. Watanabe, H. Takaya, T. Haino, N. Yasuda, S. Yamago, *Chem. – Eur. J.* **2013**, *19*, 14061–14068.
- [100] T. Iwamoto, Z. Slanina, N. Mizorogi, J. Guo, T. Akasaka, S. Nagase, H. Takaya, N. Yasuda, T. Kato, S. Yamago, *Chem. – Eur. J.* **2014**, *20*, 14403–14409.
- [101] H. Ueno, T. Nishihara, Y. Segawa, K. Itami, *Angew. Chem. Int. Ed.* **2015**, *54*, 3707–3711.
- [102] Q. Huang, G. Zhuang, H. Jia, M. Qian, S. Cui, S. Yang, P. Du, *Angew. Chem. Int. Ed.* **2019**, *58*, 6244–6249.
- [103] D. Lu, Q. Huang, S. Wang, J. Wang, P. Huang, P. Du, *Front. Chem.* **2019**, *7*, DOI 10.3389/fchem.2019.00668.

- [104] Y. Xu, B. Wang, R. Kaur, M. B. Minameyer, M. Bothe, T. Drewello, D. M. Guldi, M. von Delius, *Angew. Chem. Int. Ed.* **2018**, *57*, 11549–11553.
- [105] J. C. Sancho-García, M. Moral, A. J. Pérez-Jiménez, *J. Phys. Chem. C* **2016**, *120*, 9104–9111.
- [106] E. Kayahara, L. Sun, H. Onishi, K. Suzuki, T. Fukushima, A. Sawada, H. Kaji, S. Yamago, *J. Am. Chem. Soc.* **2017**, *139*, 18480–18483.
- [107] J. B. Lin, E. R. Darzi, R. Jasti, I. Yavuz, K. N. Houk, *J. Am. Chem. Soc.* **2019**, *141*, 952–960.
- [108] S. Wang, X. Li, G. Zhuang, M. Chen, P. Huang, S. Yang, P. Du, *Chem. Commun.* **2021**, *57*, 9104–9107.
- [109] H. Sakamoto, T. Fujimori, X. Li, K. Kaneko, K. Kan, N. Ozaki, Y. Hijikata, S. Irlle, K. Itami, *Chem. Sci.* **2016**, *7*, 4204–4210.
- [110] T. A. Schaub, E. A. Prantl, J. Kohn, M. Bursch, C. R. Marshall, E. J. Leonhardt, T. C. Lovell, L. N. Zakharov, C. K. Brozek, S. R. Waldvogel, S. Grimme, R. Jasti, *J. Am. Chem. Soc.* **2020**, *142*, 8763–8775.
- [111] R. Frydrych, K. Senthilkumar, K. Ślusarek, M. Waliczek, W. Bury, P. J. Chmielewski, J. Cybińska, M. Stępień, *Org. Chem. Front.* **2025**, *12*, 437–447.
- [112] S. Wang, X. Li, X. Zhang, P. Huang, P. Fang, J. Wang, S. Yang, K. Wu, P. Du, *Chem. Sci.* **2021**, *12*, 10506–10513.
- [113] Y. Fan, S. Fan, L. Liu, S. Guo, J. He, X. Li, Z. Lian, W. Guo, X. Chen, Y. Wang, H. Jiang, *Chem. Sci.* **2023**, *14*, 11121–11130.
- [114] D. Chen, Y. Wada, Y. Kusakabe, L. Sun, E. Kayahara, K. Suzuki, H. Tanaka, S. Yamago, H. Kaji, E. Zysman-Colman, *Org. Lett.* **2023**, *25*, 998–1002.
- [115] H. Tang, Z. Gu, C. Li, Z. Li, W. Wu, X. Jiang, *Biomater. Sci.* **2019**, *7*, 2552–2558.
- [116] D. Imoto, H. Shudo, A. Yagi, K. Itami, *Angew. Chem. Int. Ed.* **2025**, *64*, e202413828.
- [117] X. Li, L. Jia, W. Wang, Y. Wang, D. Sun, H. Jiang, *J. Mater. Chem. C* **2023**, *11*, 1429–1434.
- [118] Z.-A. Huang, C. Chen, X.-D. Yang, X.-B. Fan, W. Zhou, C.-H. Tung, L.-Z. Wu, H. Cong, *J. Am. Chem. Soc.* **2016**, *138*, 11144–11147.
- [119] P. J. Evans, L. N. Zakharov, R. Jasti, *J. Photochem. Photobiol. Chem.* **2019**, *382*, 111878.
- [120] T. Ide, W.-C. Huang, M. Horie, *J. Am. Chem. Soc.* **2024**, *146*, 10246–10250.
- [121] N. D. MARSH*, I. PRECIADO, E. G. EDDINGS, A. F. SAROFIM, A. B. PALOTAS, J. D. ROBERTSON, *Combust. Sci. Technol.* **2007**, *179*, 987–1001.
- [122] M. Almanzalawy, S. Nada, A. Elwardany, M. Elkady, *Chem. Eng. Sci.* **2025**, *303*, 120964.
- [123] X. Wang, Y. Qi, Y. Shen, Y. Yuan, L. Zhang, C. Zhang, Y. Sun, *Sens. Actuators B Chem.* **2020**, *310*, 127756.
- [124] B. Wu, S. Yeasmin, Y. Liu, L.-J. Cheng, *Sens. Actuators B Chem.* **2022**, *354*, 131216.
- [125] L. Cunningham, A. Benson, P. J. Guiry, *Org. Biomol. Chem.* **2020**, *18*, 9329–9370.
- [126] D. Golagani, S. Ajmeera, W. Erb, F. Mongin, S. Murthy Akondi, *Chem. Commun.* **2023**, *59*, 9259–9262.
- [127] E. Payami, A. Mohammadzadeh, K. D. Safa, R. Teimuri-Mofrad, *J. Energy Storage* **2024**, *88*, 111624.
- [128] M.-L. Hu, M. Abbasi-Azad, B. Habibi, F. Rouhani, H. Moghanni-Bavil-Olyaei, K.-G. Liu, A. Morsali, *ChemPlusChem* **2020**, *85*, 2397–2418.
- [129] K. E. Lewis, G. P. Smith, *J. Am. Chem. Soc.* **1984**, *106*, 4650–4651.
- [130] D. Astruc, *Eur. J. Inorg. Chem.* **2017**, *2017*, 6–29.
- [131] T. Muraoka, K. Kinbara, Y. Kobayashi, T. Aida, *J. Am. Chem. Soc.* **2003**, *125*, 5612–5613.
- [132] T. Muraoka, K. Kinbara, T. Aida, *Nature* **2006**, *440*, 512–515.

Chapter 1

- [133] C. Xiao, W. Wu, W. Liang, D. Zhou, K. Kanagaraj, G. Cheng, D. Su, Z. Zhong, J. J. Chruma, C. Yang, *Angew. Chem. Int. Ed.* **2020**, *59*, 8094–8098.
- [134] N. Kubota, Y. Segawa, K. Itami, *J. Am. Chem. Soc.* **2015**, *137*, 1356–1361.
- [135] E. Kayahara, V. K. Patel, A. Mercier, E. P. Kündig, S. Yamago, *Angew. Chem. Int. Ed.* **2016**, *55*, 302–306.
- [136] J. M. Van Raden, S. Louie, L. N. Zakharov, R. Jasti, *J. Am. Chem. Soc.* **2017**, *139*, 2936–2939.
- [137] M. J. H. Ojea, J. M. V. Raden, S. Louie, R. Collins, D. Pividori, J. Cirera, K. Meyer, R. Jasti, R. A. Layfield, *Angew. Chem. Int. Ed.* **2021**, *60*, 3515–3518.
- [138] B. Lan, J. Xu, L. Zhu, X. Chen, H. Kono, P. Wang, X. Zuo, J. Yan, A. Yagi, Y. Zheng, S. Chen, Y. Yuan, K. Itami, Y. Li, *Precis. Chem.* **2024**, *2*, 143–150.
- [139] P. J. Fagan, M. D. Ward, J. C. Calabrese, *J. Am. Chem. Soc.* **1989**, *111*, 1698–1719.
- [140] A. A. Kamin, T. D. Clayton, C. E. Otteson, P. M. Gannon, S. Krajewski, W. Kaminsky, R. Jasti, D. J. Xiao, *Chem. Sci.* **2023**, *14*, 9724–9732.